

# Influence of HSM cutting parameters on the surface integrity characteristics of hardened AISI H13 steel

Daniel Hioki · Anselmo E. Diniz · Amilton Sinatora

Received: 23 May 2012 / Accepted: 19 November 2012 / Published online: 7 July 2013  
© The Brazilian Society of Mechanical Sciences and Engineering 2013

**Abstract** The purpose of this study is to evaluate the influence of the cutting parameters of high-speed machining milling on the characteristics of the surface integrity of hardened AISI H13 steel. High-speed machining has been used intensively in the mold and dies industry. The cutting parameters used as input variables were cutting speed ( $v_c$ ), depth of cut ( $a_p$ ), working engagement ( $a_e$ ) and feed per tooth ( $f_z$ ), while the output variables were three-dimensional (3D) workpiece roughness parameters, surface and cross section microhardness, residual stress and white layer thickness. The subsurface layers were examined by scanning electron and optical microscopy. Cross section hardness was measured with an instrumented microhardness tester. Residual stress was measured by the X-ray diffraction method. From a statistical standpoint (the main effects of the input parameters were evaluated by analysis of variance), working engagement ( $a_e$ ) was the cutting parameter that exerted the strongest effect on most of the 3D roughness parameters. Feed per tooth ( $f_z$ ) was the most

important cutting parameter in cavity formation. Cutting speed ( $v_c$ ) and depth of cut ( $a_p$ ) did not significantly affect the 3D roughness parameters. Cutting speed showed the strongest influence on residual stress, while depth of cut exerted the strongest effect on the formation of white layer and on the increase in surface hardness.

**Keywords** HSM milling · H13 steel · Surface integrity · Tribology

## List of symbols

$A_r$	Real contact area
$a_p$	Depth of cut, mm
$a_e$	Working engagement, mm
$c_h$	Crest height, mm
$f_z$	Feed per tooth, mm
$v_c$	Cutting speed, m/min
$S_a$	Arithmetic mean, $\mu\text{m}$
$S_q$	Root-mean-square deviation of the surface, $\mu\text{m}$
$S_z$	Ten-point height of the surface, $\mu\text{m}$
$S_{sk}$	Asymmetry of surface deviations about the mean plane
$S_{ku}$	Peakedness or sharpness of surface height distributions
$S_{pk}$	Reduced summit height, $\mu\text{m}$
$S_k$	Core roughness depth, $\mu\text{m}$
$S_{vi}$	Valley fluid retention index
$S_{tr}$	Texture aspect ratio

Technical Editor: Alexandre Abrão.

D. Hioki (✉)  
Academic Department of Mechanics, Federal Technological  
University of Paraná, Curitiba, PR 80230-901, Brazil  
e-mail: hioki@utfpr.edu.br

A. E. Diniz  
Faculty of Mechanical Engineering, State University  
of Campinas, Campinas, SP 13083-970, Brazil  
e-mail: anselmo@fem.unicamp.br

A. Sinatora  
Laboratory of Surface Phenomena, Department of Mechanical  
Engineering, Polytechnic School of the University of São Paulo,  
São Paulo, SP 05508-900, Brazil  
e-mail: sinatora@usp.br

## 1 Introduction

According to Dewes et al. [11], high-speed machining (HSM) was introduced by Carl Salomon in 1931, in a

patent filed by the German company Friedrich Krupp A.G. The first record of the industrial application of HSM was in the aeronautical and aerospace industry in the late 1970s.

Currently, due to market needs for diversified industrial products and the increasingly short life cycle of these products, the industry has developed systems for agile manufacturing, producing parts only in response to confirmed orders and in the amounts ordered. This worldwide trend led to the emergence of the mold and die industry to meet this new reality. The solution was to seek efficient and successful results for agile manufacturing systems and to extend flexibility to the limit without reducing productivity. Therefore, HSM has been used intensively in the mold and dies industry.

It can be defined as a milling process typically used in semi finishing and finishing operations of dies and molds where working engagement ( $a_e$ ) and depth of cut ( $a_p$ ) are very small (much smaller than the typical values used in milling) and, consequently, the ratio ( $a_e/D - D = \text{tool diameter}$ ) is also very small. Therefore, the contact angle between cutting edge and workpiece in each tool revolution is very small, preventing the tool temperature to increase so much, which makes possible the use of higher cutting speed than that typically used for milling of hardened steels, the typical material of dies and molds. Also, because  $a_e/D$  is small, the average chip thickness ( $h_m$ ) is very small, which makes possible the use of high values of feed per tooth (higher than the values typically used in finish milling) without damaging the surface roughness.

Despite having diameter much bigger than  $a_e$ , the tool is small to copy the small radius of the machined part. Therefore, due to its small diameter and the high cutting speed, tool revolution must be very high. Due to the high feed per tooth and high tool revolution, feed velocity is also very high. That is the reason why it is called HSM—high tool revolution and high feed velocity [28].

The area of machining has concentrated its efforts for many years on issues such as the volume of material removed per unit of time, tool life and geometric tolerances. In recent decades, because of the need to reduce costs, the application of engineering has increased significantly and has thus required greater component reliability. Therefore, in addition to the issues traditionally addressed in the area of machining, it is essential to evaluate the effects of machining on the performance of parts, which begins with the characterization of surface integrity.

The analysis of machined surface integrity was first proposed by Field and Kales [15] in 1964. This activity describes and assesses conditions of the surface and the layers below it. Moreover, it is a powerful tool to understand how these conditions may affect the performance of the manufactured surface, as reported by Griffiths [18] and Stout [30].

Stout and Blunt [31] proposed a classification of manufactured surfaces based on topographic characteristics and subsurface layers (Table 1).

Traditionally, the literature shows the evaluation of the condition of the surface by two-dimensional (2D) profilometry and, more recently, by three-dimensional (3D) profilometry. The condition of the surface, which can be understood as the topography or texture of the surface, is a concept that can be quantified using roughness parameters. Several studies report the utilization of 3D roughness parameters to represent the area. Hutchings [20] described the changes of topography characteristics due to different machining processes. Griffiths [18] commented that, due to the nature of surface topography, the roughness parameters show high dispersion which may be minimized by 3D measurement techniques. Mancuso [22] shows the effects of cavitation erosion through 3D parameters.

The evaluation of subsurface layers involves the use of several methods, since the energy introduced by machining leads to alterations of mechanical and metallurgical properties. Typically, the methods used to assess or quantify the subsurface characteristics are: optical and scanning microscopy, EDS and EDX, metallography, microhardness, residual stress and resistance to fracture. For special cases, Field et al. [16] proposed the evaluation of engineering properties such as: wear resistance, sealing, etc.

Several studies have established the relationship of cutting parameters ( $v_c$ ,  $a_p$ ,  $a_e$ ,  $f_z$ ) with roughness parameters and changes in the subsurface layers. Axinte and Dewes [3] performed machining tests on hardened hot work tool steel (AISI H13  $\approx 50$  HRC) using carbide ball nose end mills with TiAlN coating. The influence of cutting parameters on microhardness, residual stress, microstructure and the Ra roughness parameter were analyzed. No white layer or microstructural alterations were observed. Chevrier et al. [10] reported the effect of cutting parameters on residual stress during high-speed milling of low alloy steel (AISI 4140  $\approx 175$  HV) with carbide tool coated with TiAlN. They concluded that residual stress is usually tensile at the surface and then becomes compressive. The main reason for the stress gradient is the thermal effect. El-Wardany et al. [13] investigated the influence of hard turning of tool steel (D2  $\approx 60$  HRC) with PCBN tools and discussed surface defects, plastic deformation and microstructural alterations. However, few studies have attempted to establish, statistically, the most important factors that influence the various characteristics of surface integrity, and particularly 3D roughness parameters ( $S_a$ ,  $S_q$ ,  $S_z$ ,  $S_{sk}$ ,  $S_{ku}$ ,  $S_{pk}$ ,  $S_k$ ,  $S_{vi}$ , and  $S_{tr}$ ).

Many engineering considerations involving contact between bodies are based on macro geometry, i.e., on body contour. However, in practice, contact occurs at points located inside the area defined by the body's contour. The

**Table 1** Surface classification (adapted from [31])

Surface classification			
<b>Engineered surface</b> Surfaces produced in specific ways that deliberately alter surface and subsurface layers to give a specific functional performance		<b>Non-engineered surfaces</b> Surfaces produced as a direct consequence of the manufacturing process, where little or no attempt is made to influence surface characteristics	
<b>Structured surfaces</b> Surfaces with a deterministic pattern of usually high aspect ratio geometric features designed to give a specific function	<b>Unstructured surfaces</b> Surfaces where a deliberate attempt has been made to impart texture through semi-control of the manufacturing process without achieving a deterministic pattern	<b>Random surfaces</b> Surfaces produced by random and pseudo-random processes, often with the specific intention of removing systematic features	<b>Systematic surfaces</b> Surfaces exhibiting some repetitive features which are a consequence of the natural constraints of the process by which they have been produced
<b>Directional surfaces</b> Surfaces with a deterministic pattern which exhibits specific directionality			
<b>Non-directional surfaces</b> Surfaces with a deterministic pattern but without specific directionality			

sum of individual areas of contact is called the “real contact area”, while the area defined by the body contour is called the “apparent contact area” (Fig. 1).

Several early studies emphasize the importance of surface roughness characteristics, quantified by roughness parameters, on the number of contacts between surfaces and, consequently, how they affect some engineering properties. Boeschoten and Van Der Held [5] report the effect of contact spots on thermal conductivity between aluminum and other metals. Cao et al. [9] report the effect of surface roughness on gas flow in microfluidic devices. Uppal and Probert [33] show the correlation between surface roughness of the contacting surfaces and static contact

resistance. Magri et al. [21] tested AISI H13 (56 HRC) machined surfaces with HSM during hot forging. They proved that engineered surface, structured and non-directional with cavities formed by  $v_c = 150$  m/min,  $f_z = 0.25$  mm and  $a_e = 0.30$  mm (condition 1), showed higher wear resistance. In this work, cutting velocity and depth cut were not investigated, so the effect of these cutting parameters on surface integrity cannot possibly be estimated. The values of 3D roughness parameters of condition 1 obtained by Magri et al. [21] are very similar to those obtained on condition 10 in this work.

AISI H13 steel is widely used in the manufacture of plastic injection molds, pressure casting dies, forging, stamping, hot cutting plates, extrusion tools, etc. The manufacture of molds and dies is a lengthy process that requires special techniques involving high costs. Moreover, the method used to manufacture them affects surface integrity. Thus, to observe changes on mold and die surfaces caused during manufacturing, the same methodology was applied to manufacture the samples whose surfaces were analyzed here. This involved the use of AISI H13 steel and HSM milling to understand the influence of cutting parameter on the characteristics of surface integrity of hardened AISI H13.

Magri et al. [21] showed by tests of forging dies the importance of the surface texture. The tests were carried out in specially prepared presses and small dies were machined under different conditions to obtain distinct textures. They produced up to 125 parts in each die to evaluate the die wear. This number of parts is much lower than the number usually used in industries to reach the end of the die life; however, these experiments were very time consuming and raised the cost of research. This work paves the way to validate tribometers to simulate the main wear mechanisms that occur in machined surfaces, such as in

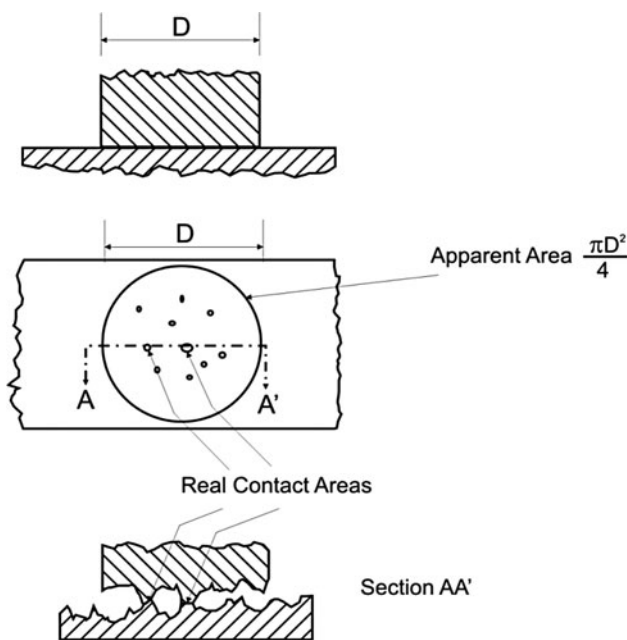


**Fig. 1** Contacts between surfaces [4]

forging dies. The tests in tribometers allow a reduction of cost and research time. However, success depends on firstly the characterization of the elements of surface integrity, in sequence, determination of wear mechanism dominant in the forging process and finally validation of it in a tribometer. Analyzes of this type allow the building of strategies to set and/or adjust manufacturing engineered surfaces which can withstand the demands of different projects.

## 2 Materials and experimental procedures

The samples used in the experiments were cut from an AISI H13 forged block (VH13-IM—Villares Metals). The chemical composition of this material is shown in Table 2.

The hardness of six randomly selected heat-treated samples was measured (three measurements of each sample). The average hardness was  $HV\ 30\ 565 \pm 5$  for a total of 18 measurements.

The machine tool used to produce the surfaces was a CNC machining center Deckel Maho DMC 63 V, maximum spindle rotation 10,000 rpm and main motor power 11 kW.

The samples were assembled in a special fixation device, which provided an angle of  $75^\circ$  between the table and the machined surface, as can be seen in Fig. 2.

The tool used in the experiments was a ball nose end mill (16 mm diameter) supplied by Sandvik. The specifications of the tool holder were R216F-16A16S-063 and those of the carbide inserts were R216F-16 40 class P20A (recommended for materials with hardness up to HV 590).

The  $v_c = 150$  m/min was adopted as recommended by the tool manufacturer (75–190 m/min) Sandvik [27]. The speed of 300 m/min was selected to investigate its effect on surface integrity.

The relation between “crest height— $c_h$ ” and  $a_e$  can be defined by Eq. (1):

$$c_h = \frac{a_e^2}{8R} \quad (1)$$

where  $R$  is the radius of the tool used. This work adopted crest heights of 0.002 and 0.014 mm. As a result, the  $a_e$  used were 0.35 and 0.95 mm.

The  $a_p$  followed the manufacturer’s recommendation which states that it should not exceed  $0.03 \times$  “contact

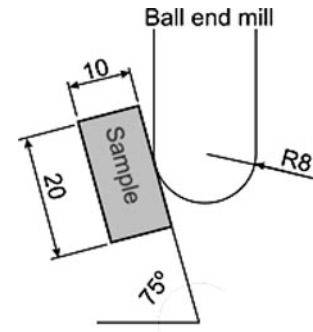


Fig. 2 Schematic drawing of the sample in relation to the table

diameter”. As shown in the figure, the contact diameter was approximately 15 mm. Thus,  $a_p < 0.45$  mm.

The machining conditions followed the tool manufacturer’s recommendations, as presented in Table 3. Fractional factorial design was used in this work.

The experiments were performed dry and a flow of compressed air was injected close to the tool to expel the chips.

A fresh cutting edge was used for each machining condition. The milling method adopted was contour, upward and down (or climb) milling.

### 2.1 Characterization of surface integrity

#### 2.1.1 Topographic characterization

Topographic characterization consisted of measuring the 3D roughness in the direction perpendicular to the feed of the milling tool using a 3D profilometer—UBM Mess-technik. In this work, the measured area was  $4 \times 4$  mm at 0.001 mm intervals along each profile. The collected data were analyzed using the “Mountain map version 3.0.11” software.

#### 2.1.2 Microhardness measurements

An instrumented microhardness, Fischer scope HCV HV 100 tester, was used, with load of 100 mN. Before taking the measurements, the surfaces were polished with  $1 \mu\text{m}$  diamond paste. To obtain the hardness profile of the transverse section of the samples, indentations were made below the machined surface at distances of 0.03, 0.05, 0.1,

Table 2 Chemical composition of AISI H13 steel

C	Si	Mn	P	S	Co	Cr	Mo	Ni	V	W	Cu	Al
0.39	1.11	0.28	0.019	0.001	0.06	5.09	1.33	0.25	0.81	0.06	0.1	0.02

Values in percentage weight

**Table 3** Cutting parameters of the experiments, matrix  $2^{4-1}$

Condition	$v_c$ (m/min)	$a_p$ (mm)	$a_e$ (mm)	$f_z$ (mm)
1	150	0.2	0.35	0.05
4	300	0.4	0.35	0.05
6	150	0.2	0.95	0.05
7	300	0.4	0.95	0.05
10	150	0.2	0.35	0.25
11	300	0.4	0.35	0.25
13	150	0.2	0.95	0.25
16	300	0.4	0.95	0.25

0.2, 0.3, 0.4 and 0.5 mm. Each value shown in Sect. 3 represents the average of 15 measurements.

To measure microhardness on the machined surface, the samples were polished for only 10 s. This sufficed to generate a flat region on which to measure the microhardness. In this stage, 30 measurements were taken from each sample due to the wide dispersion of hardness values.

### 2.1.3 White layer measurement

To measure the thickness of the white layer, the samples were etched with Vilella reagent for 10 s and examined with an optical microscope, Olympus BX60 and Scanning Electron Microscope, Philips XL 30. Each value corresponds to an average of three measurements of the maximum value of the layer thickness.

### 2.1.4 Residual stress measurement

This parameter was examined using an X-ray diffractometer, Rigaku Rint 2000. The measurements were based on the constants shown in Table 4.

A region was selected in each sample and 13 residual stress measurements were taken by changing the angle (discrete values at  $10^\circ$  intervals) and the mean and standard deviation of the measured values was recorded. Residual stress measurements were taken only on the machined surfaces. The residual stress profile in the transverse section was not investigated.

**Table 4** Characteristics of residual stress measurements

Constants	
$E$	210,000 MPa
$\delta$	0.29
Plane	211
Target	Cr ( $k$ -alpha)
Aperture	$2 \times 2$ mm
Feed	0.04°/min
Scan angle ( $\theta$ )	152–157.5

### 2.1.5 Analysis of the results

The analysis of variance (ANOVA) method is based on partitioning the total variance of a given response (dependent variable) into suitable components (mean variation and residual variation). The ANOVA  $F$  test determines the difference between the means. An independent variable (cutting parameter) with a calculated  $F$  ( $F_{calc}$ ) higher than the tabulated value of  $F$  indicates a significant influence on the dependent variable (roughness parameters, residual stress, white layer, etc.). The results obtained for each 3D roughness parameter and their replicate are in “Appendix”, Table 12. The ANOVA tables for each dependent variable, containing the values of  $F_{calc}$ , are shown in the “Appendix”. In this paper, the number of replicates was two and the significance level adopted was 0.05. Only the influence of the cutting parameter with the most significant statistical effect on the roughness parameter was analyzed.

## 3 Results and discussion

The photographs of surfaces in Fig. 3 were taken using a microscope with radial lighting,  $10\times$  magnification and a  $22.5^\circ$  angle of incidence of the light beam.

The predominant topography of the surfaces of group A (upper row of photographs in Fig. 3, conditions 1, 4, 6, 7) consists of parallel valleys separated by mountain ranges, regions in which the summits are apparently continuous. This kind of topography was caused by the low feed per tooth ( $f_z = 0.05$  mm) used in these conditions, which resulted in a much lower roughness in the feed direction than in the direction perpendicular to the feed. Note, also, that the distances between the valleys in conditions 1 and 4 ( $a_e = 0.35$  mm) are smaller than in conditions 6 and 7 ( $a_e = 0.95$  mm).

The topography of the surfaces of group B (lower row of photographs in Fig. 3, conditions 10, 11, 12, 16) consists of a regular arrangement of depressions and cavities. These cavities appear to have a circular geometry in conditions 10 and 11.

At higher values of feed per tooth, the roughness in both directions (perpendicular and parallel to the feed) becomes similar. Engineered surfaces, structured and non-directional, conditions 10 and 11, were obtained when the  $a_e$  values approached the  $f_z$  values, since feed per tooth value is the most influent variable on roughness in the feed direction and  $a_e$  value is the most influent variable on roughness in the direction perpendicular to the feed.

As Fig. 4 shows, in condition 6 the topography consists of valleys and summits that make up the periodic wave (mountain range) caused by the translational movement of

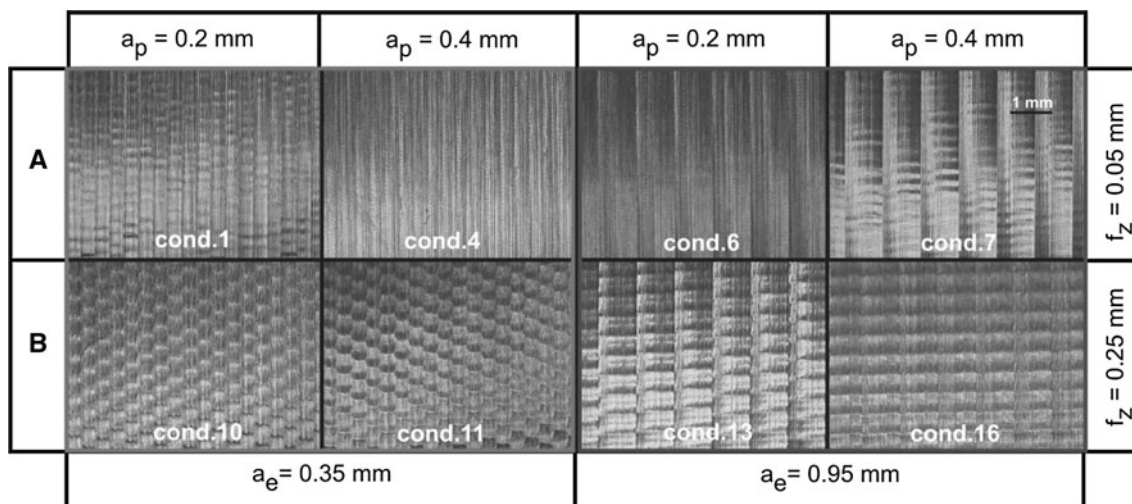


**Fig. 3** Milled surfaces at  $\times 10$  magnification

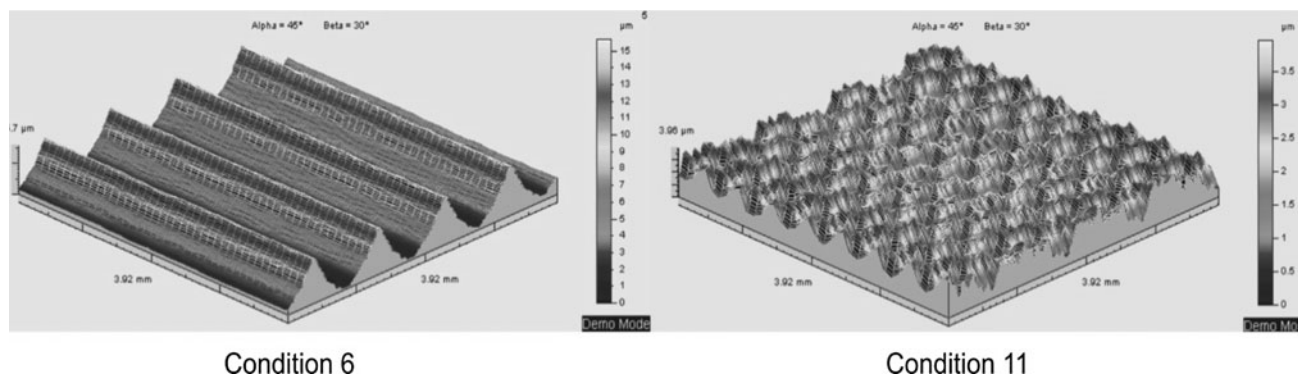


**Fig. 4** Results of the profilometry measurements of conditions 6 and 11

the mill in the feed direction, and in condition 11, the cavities show a regular arrangement.

The real contact area ( $A_r$ ) between an ideal plane and a real surface when high loads are used can be calculated by Eq. (2) (Fig. 5).

$$A_r = A \times c \times N \quad (2)$$

where  $A$  length of waviness at  $Y$  axis,  $c$  width of the highest part of the waviness due to plastic deformation,  $N$  number of waves on the  $X$  axis.

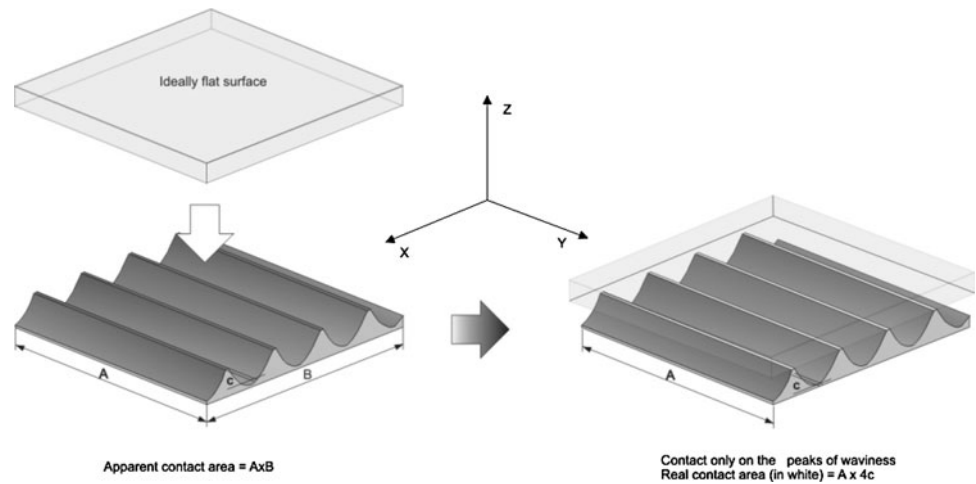
Thus, if a surface like the one obtained with condition 6 comes into contact with an ideally plane surface, the contact will occur at the highest peaks located on the summits of waves and along the  $Y$  axis (see Fig. 5). In other words, to determine how the contact will occur requires considering the apparent area of contact and its relationship with the machined topography or, in the case of condition 6, how many waves and what length should be considered within the apparent contact area.

These comments about the importance of waviness parameters in real contact analysis between bodies, though

obvious, give rise to new considerations about the importance of these parameters, since wave values are often filtered out during traditional roughness analyses, as recommended by the ASME B46.1-2002 and NBR ISO 4287:2002 [2, 8].

This recommendation to filter out waviness signals may have originated during the development of the device to measure the asperity level, e.g., see Firestone et al. [17]. At that time, the objective was either the finishing specification of pieces according to their applications or to meet the surface design requirements in manufacturing processes. Abbott and Arbor [1] stated that the profiles that make up the surface are complex, composed of waves with different intensities and lengths that represent the irregularities produced in the machining process. Thus, it was desirable to measure the topography separately, by electrical circuit (wave filters), to study the effect of changing the surface machining method, i.e., to measure the effect of cutting parameters on different topographic characteristics. Whitehouse and Mowbray [35], Starr and Reeve [29] and others improved the waviness profile filtering technique without distorting the roughness profile.

**Fig. 5** Contact of machined surface with an ideally plane surface



As mentioned earlier, some properties (wear, heat transfer) are affected by the “real contact area”. Thus, it is necessary to analyze the primary profile to consider waviness and roughness. Therefore, in this work, the primary profile described by Trumpold and Heldet [32] was used for the topographic analysis.

In applications involving contact between two bodies, their tribological performance will be determined by forces (strength and speed of deformation), the environment (temperature, humidity, contamination and lubricants), the materials of the two bodies (microstructure, hardness, residual stress and mechanical properties) and surface texture. With regard to texture, the important roughness parameters are the ones that determine the real area of contact, the bearing capability, and those that determine lubricant retention and leakage. In the classical literature on tribology, the important parameters for determining the real area of contact are density summits, slope of the asperities and their radius, which limit the study of contacts at loads that affect only the topography at the roughness level. For high loads, one must consider another scale (topography and waviness), which is the approach adopted in this work. The bearing capacity, a property that indicates the end of the localized flow, and the oil retention capacity are functional parameters that were studied here. An examination of Fig. 2 reveals that the directionality of the texture should be considered in the study of the contact. In this work, the directionality was studied using the  $S_{tr}$  parameter.

### 3.1 Influence of work engagement ( $a_e$ ) on the amplitude parameter

The ANOVA results (Table 5 in the “Appendix”) confirm that work engagement ( $a_e$ ) is the cutting parameter with the strongest statistical effect on the amplitude roughness parameter ( $S_a$ ) measured orthogonally to the feed direction. This roughness parameter increases with the work engagement (Fig. 6).

The reason for this influence is that, with increasing work engagement ( $a_e$ ), the width and depth of grooves on the primary profile also increase.

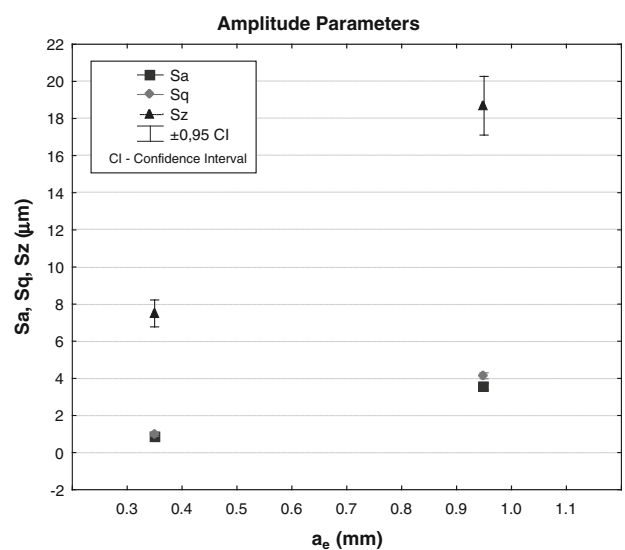


**Fig. 6** Influence of work engagement ( $a_e$ ) on the amplitude parameters

Consequently, the deviation of amplitudes of surface asperities distributed on the surface waviness ( $S_q$ ) and the distances between peaks and valleys ( $S_z$ ) will be higher. The measured roughness values are consistent with those reported by other researchers (Fallböhmer [14], Urbanski et al. [34]). This group of roughness parameters increases with work engagement.

### 3.2 Influence of work engagement ( $a_e$ ) on amplitude distribution parameters

The ANOVA (Table 6 in the “Appendix”) confirms that work engagement ( $a_e$ ) is the cutting parameter with the greatest statistical effect on amplitude distribution parameters. The graph in Fig. 7 shows the influence of  $a_e$  on skewness ( $S_{sk}$ ) and kurtosis ( $S_{ku}$ ). These two roughness parameters showed the opposite behavior. At the lowest  $a_e$

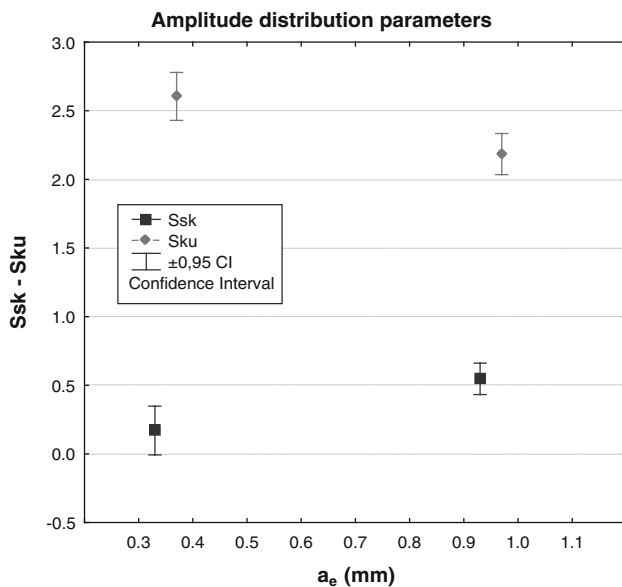


**Fig. 7** Influence of work engagement ( $a_e$ ) on  $S_{sk}$  and  $S_{ku}$

value, a combination of skewness close to zero and kurtosis close to three occurred. When  $a_e$  increased, skewness increased and kurtosis decreased.

The amplitude distribution curves of conditions 6, 4 and 11 (Fig. 8) help to clarify the practical meaning of this result. In condition 6 (Fig. 8), the amplitudes that presented the highest frequency are above the reference plane (12.4  $\mu\text{m}$  from the surface, skewness— $S_{sk}$  positive). Furthermore, the curve of condition 6 is flatter (low kurtosis— $S_{ku}$ ) than the others. In condition 11, the amplitudes with the highest frequency are very close to the reference plane (at 3.97  $\mu\text{m}$  from the surface, skewness— $S_{sk}$  tends to zero). The reason for this is that the decrease in work engagement ( $a_e$ ) generated a primary profile with lower waviness and, consequently, the distribution of roughness peaks was more concentrated, resulting in a high kurtosis. Although conditions 11 and 4 have low values of  $S_q$ , condition 11 has asymmetry tending to zero and condition 4 has a positive  $S_{sk}$ . The reason is that, for condition 11, the amplitude of waviness in the feed tool direction was close to that of the transverse waviness, which is easily visualized in the graphic representation of surface in Fig. 4. Therefore, in condition 11, the frequency of amplitude close to the surface is higher than in condition 4 and its asymmetry tends to zero.

### 3.3 Influence of work engagement ( $a_e$ ) on functional parameters

The ANOVA (Table 7 in the “Appendix”) confirms that work engagement ( $a_e$ ) is the cutting parameter with the greatest statistical effect on functional parameters. The graph in Fig. 9 shows that the functional parameters  $S_{pk}$  and  $S_k$  increased with work engagement ( $a_e$ ).

Comparing the primary profiles of conditions 4 and 6 (Figs. 10, 11), it can be observed that the increase in work engagement ( $a_e$ ) promoted increased wave amplitudes above the mean plane of the primary profile and also augmented the slope of the Abbott curve in relation to the horizontal axis (Fig. 12). These two factors caused an increase in the region of peaks ( $S_{pk}$ ) (Fig. 12).

The  $S_k$  parameter is related to the smallest vertical distance between two points spaced at 40 % on the  $X$  axis of the Abbott curve.

The increase in the slope of this curve, which resulted from increased work engagement ( $a_e$ ), promoted the increase of  $S_k$ .

As can be seen, in the conditions with  $a_e = 0.95$  mm, the  $S_k$  occupies much of the region situated below the mean plane. Therefore, a small statistically unrepresentative region remained for  $S_{vk}$ . Thus, the functional parameter  $S_{vi}$  was used to analyze the valley region.

The graph in Fig. 13 shows the influence of work engagement ( $a_e$ ) on the functional parameter  $S_{vi}$ —fluid retention index. This parameter is defined as the sum of the empty volumes of the valley region at 80 % on the  $X$  axis of the Abbott curve divided by  $S_q$ .

The graph shows that the fluid retention index ( $S_{vi}$ ) decreased with increasing work engagement ( $a_e$ ), because  $S_q$  increased more than the amount of empty volumes in the valley, thus reducing  $S_{vi}$ .

### 3.4 Influence of feed per tooth ( $f_z$ ) on the spatial parameters

The ANOVA (Table 8 in the “Appendix”) confirms that feed per tooth ( $f_z$ ) is the cutting parameter with the strongest statistical effect on spatial parameters.

The graph in Fig. 14 illustrates the influence of feed per tooth ( $f_z$ ) on the spatial parameter  $S_{tr}$ . According to Griffiths [18], this parameter is related to the directionality of the surface texture.

### 3.5 Alterations of the layers below the milled surface

Formation of burrs, deformation of the subsurface layers, changes in microhardness and residual stresses were observed in this study. Cracks on the machined surface were not detected. According to El-Wardany et al. [13], cracks form more frequently when machining is performed with worn tools. Therefore, since each test was performed with a fresh tool, this type of surface defect was not observed in this work.

Figure 15 shows a burr formed on a surface. This type of defect is common and tends to form on the edges of the grooves, because the thickness of the machined material near the edges tends to zero. When the chip thickness is very small, cutting no longer occurs, but the material is plastically deformed and pushed, resulting in burrs.



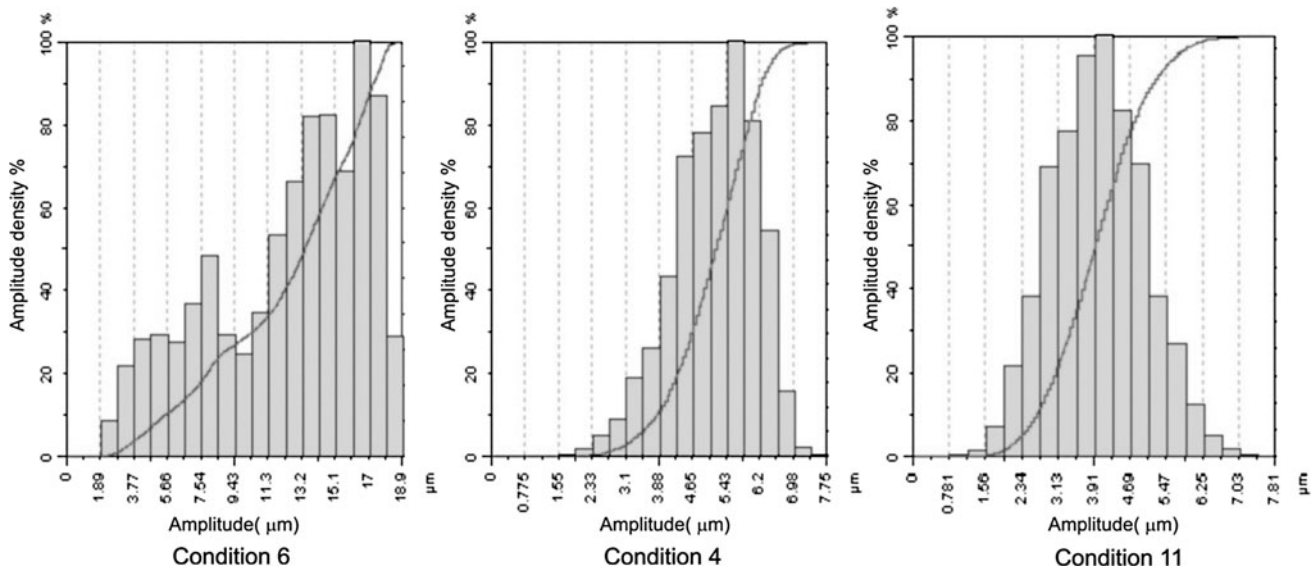


Fig. 8 Amplitude distribution function

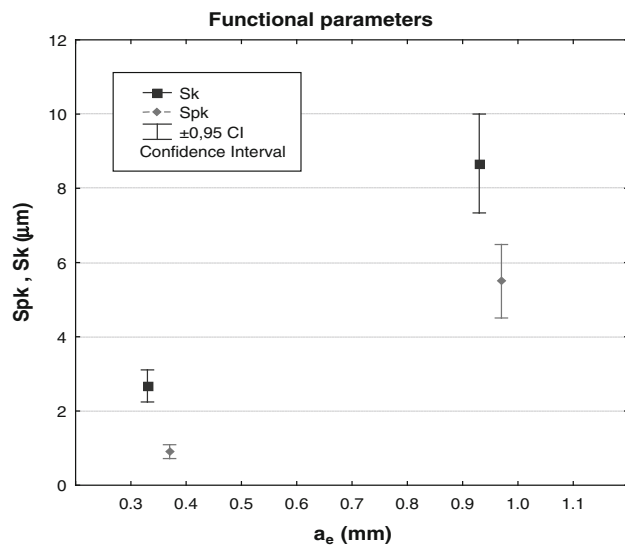


Fig. 9 Influence of work engagement ( $a_e$ ) on  $S_{pk}$  and  $S_k$

### 3.6 Influence of cutting parameters on the white layer

Figure 16 shows the white layer and the lines of deformation captured by SEM-BSE. The white layer showed a low concentration of carbides, which is consistent with the observations of Poulachon et al. [23].

The ANOVA (Table 9 in the “Appendix”) confirms that the cutting parameter exerting the strongest statistical effect on the white layer is the depth of cut ( $a_p$ ). The graph in Fig. 17 shows the influence of depth of cut ( $a_p$ ) and feed per tooth ( $f_z$ ) on the thickness of the white layer. This figure shows that the thickness of the white layer decreased with increasing feed per tooth ( $f_z$ ) and increased with the depth of cut ( $a_p$ ).

Bosheh and Mantivega [6] reported that the increase in depth of cut ( $a_p$ ) increased the volume of material removed per unit of the edge length, causing greater plastic deformation and, hence, greater white layer thickness. According to Diniz et al. [12], as the feed per tooth ( $f_z$ ) grows, chip thickness also increases, causing the cutting pressure (force per removed chip area) to decrease. Consequently, there was less plastic deformation on the machined surface and the white layer became thinner. Another explanation for this behavior may be the fact that when feed per tooth increases, the rubbing effect of the tool on the surface decreases (a cutting edge rubs less on the same portion of the machined surface).

Contrary to the results obtained in this work, Axinte and Dewes [3] did not observe white layer even in heavy conditions. However, Poulachon et al. [23] reported that, due to the nature of the white layer, special care must be taken in preparing samples. Moreover, the sample must be cut in the tool feed direction to facilitate visualization. In this study, the ANOVA showed no significant effect of cutting speed ( $v_c$ ) on the white layer.

### 3.7 Influence of cutting parameters on machined surface microhardness

In a further effort to identify the changes caused by HSM milling on the underlying layers of the machined surface, the cross section of each sample was subjected to a series of microhardness measurements. The results indicate that HSM milling did not significantly change the subsurface microhardness. Similar results are reported by Braghini [7] when machining AISI H13 (~50HRC) with TiAlN coated solid carbide ball nose end mills and by Hioki [19] when machining AISI 52100 (40–60 HRC) with PCBN inserts. This is because

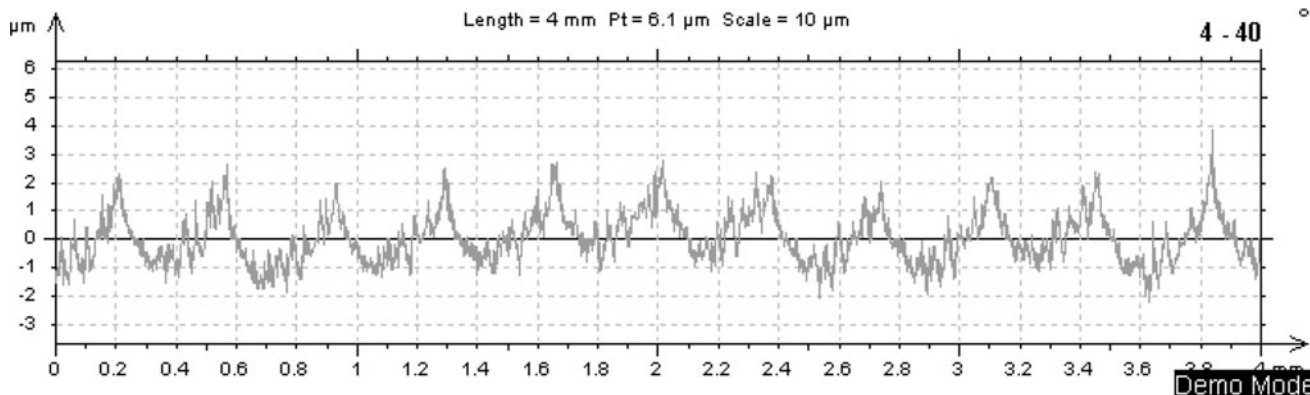


Fig. 10 Roughness profile: condition 4 ( $a_e = 0.35$  mm)

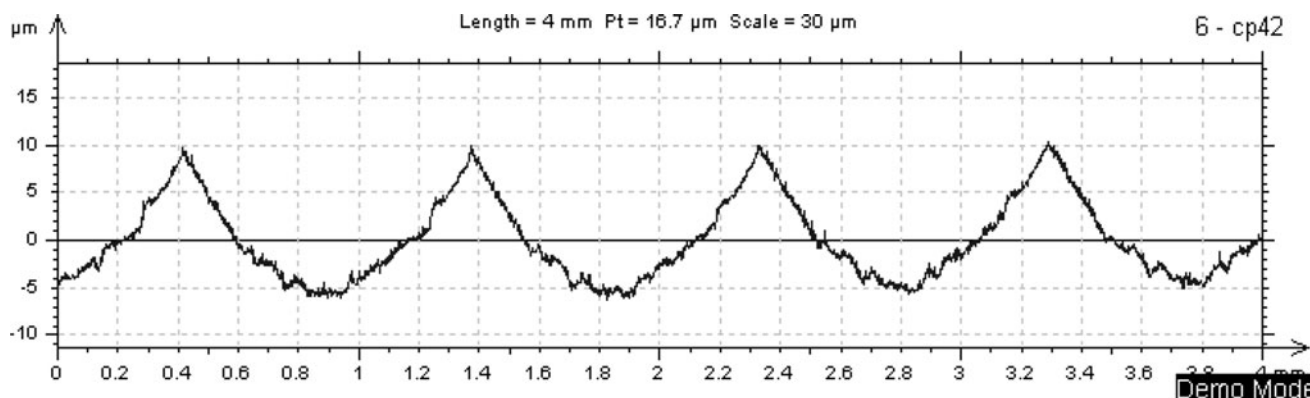


Fig. 11 Roughness profile: condition 6 ( $a_e = 0.95$  mm)

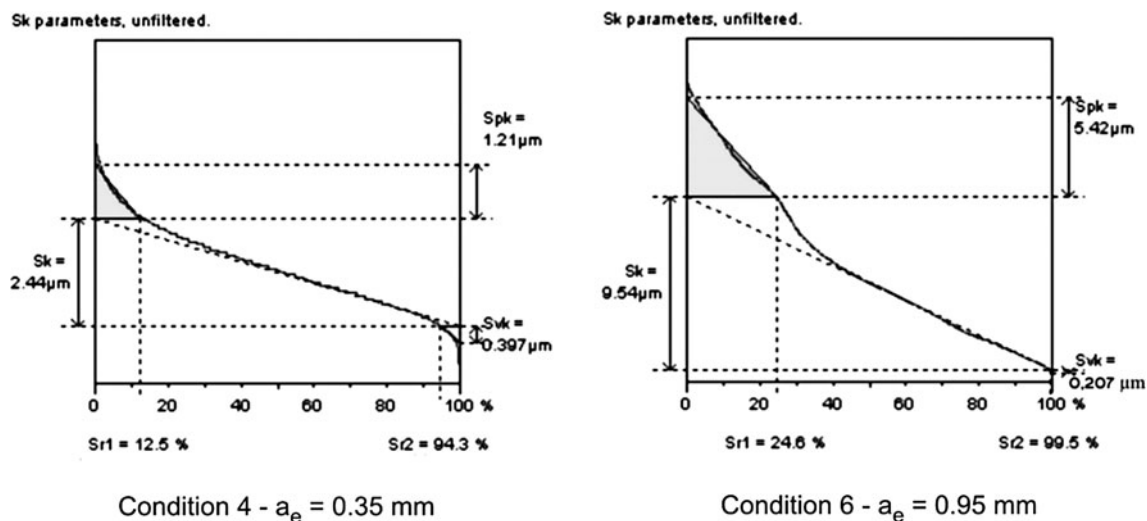
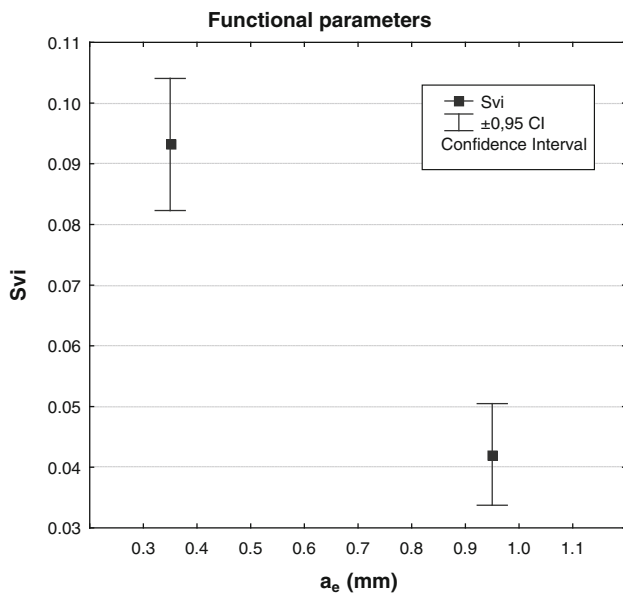


Fig. 12 Functional parameters: condition 4  $a_e = 0.35$  mm; condition 6  $a_e = 0.95$  mm

hardening, if it occurred, was located in a region smaller than the distance recommended to avoid edge deformation during hardness measurements (from 2.5 to 3 times the diagonal of the indentation  $\approx 21$   $\mu\text{m}$ ). Therefore, hardening was undetectable by this kind of measurement.

Thus, microhardness measurements had to be taken on the milled surfaces of the samples. This procedure revealed the influence of cutting conditions on surface hardness. The graph in Fig. 18 shows the influence of depth of cut ( $a_p$ ) and feed per tooth ( $f_z$ ) on surface hardness, according to the



**Fig. 13** Influence of work engagement ( $a_e$ ) on  $S_{vi}$

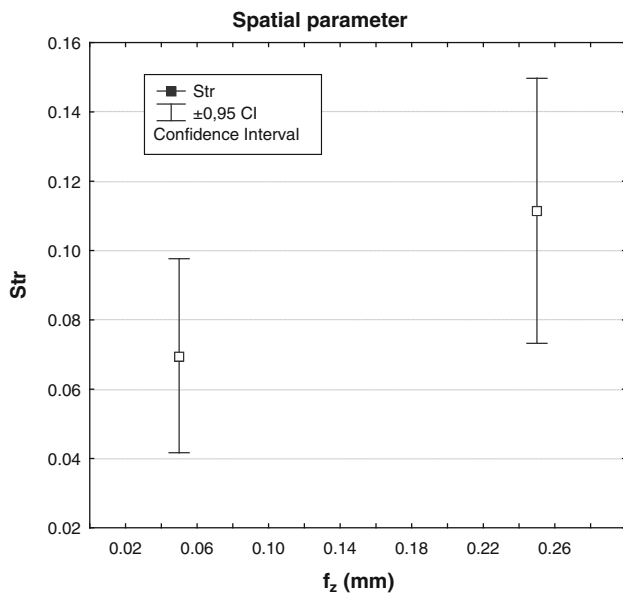


**Fig. 14** Influence of feed per tooth ( $f_z$ ) on  $S_{tr}$

ANOVA (Table 10 in the “Appendix”). The influence of cutting conditions on surface hardness was very similar to their influence on white layer thickness, i.e., hardness decreased with the increase in feed per tooth and increased with the increase in depth of cut.

There is a strong indication that the changes in the two characteristics (surface hardness and white layer) caused by the cutting conditions originated from the same source, i.e., the decrease of cutting pressure caused by the feed increase.

Regarding the effect of depth of cut ( $a_p$ ) on hardness, El-Wardany et al. [13] found contradictory results. They

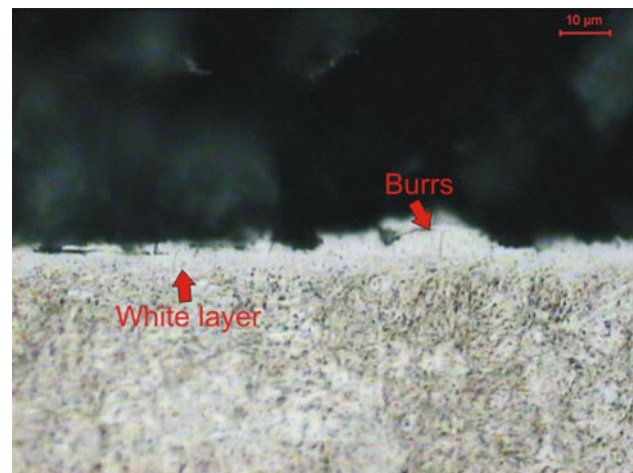


**Fig. 15** Defects on the machined surface—condition 16—feed direction

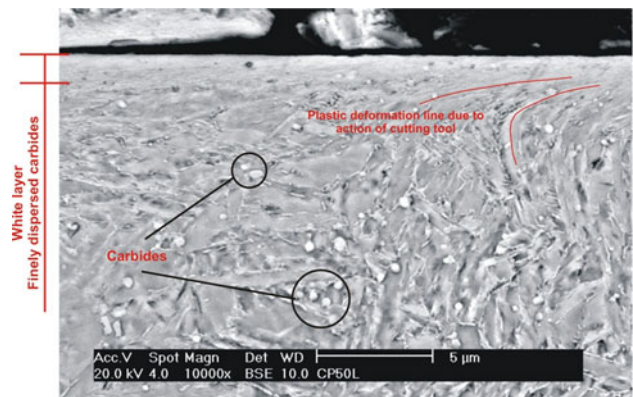


**Fig. 16** SEM micrograph of the white layer—condition 13—feed direction

reported that hardness tends to decrease with increasing depth of cut ( $a_p$ ). A possible reason for this difference is that thermal effects were probably predominant in the tests performed by these researchers. The evidence indicating the feasibility of this hypothesis is the behavior of residual stresses, which were compressive on the surface but became tensile at a shallow depth. Another point that reinforces this hypothesis is the high cutting speed ( $v_c = 350$  m/min) adopted by the aforementioned researchers. According to Rech and Moisan [25], at this level of  $v_c$ , the thermal effects begin to outweigh the mechanical effects.

In milling H13 at a cutting speed ( $v_c$ ) of 150 m/min, Braghini [7] reported that when the depth of cut ( $a_p$ ) increased from 0.1 to 0.25 mm, the stored energy (SE) in the workpiece, and hence the temperature, increased. This indicates that the thermal effects in the present study increased with the depth of cut ( $a_p$ ), but not sufficiently to promote the reduction of hardness reported by El-Wardany et al. [13].

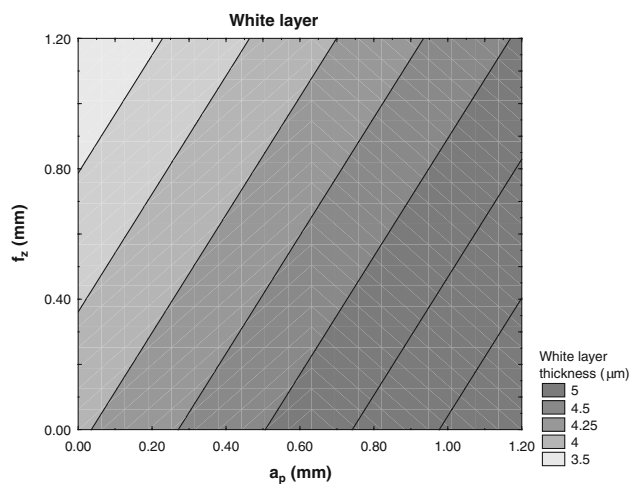


**Fig. 17** Influence of depth of cut ( $a_p$ ) and feed per tooth ( $f_z$ ) on the thickness of the white layer

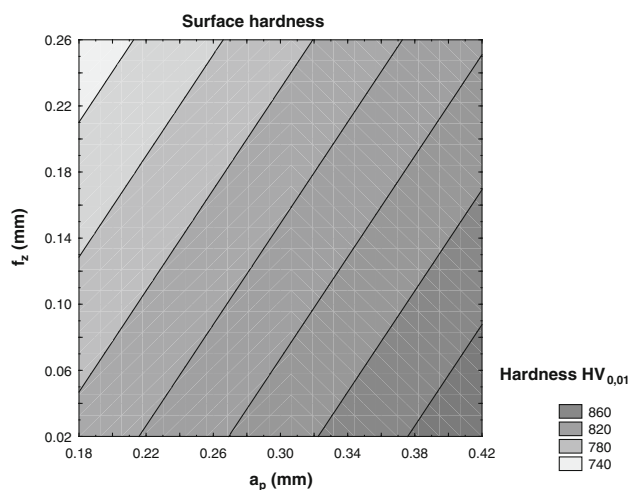


**Fig. 18** Influence of depth of cut ( $a_p$ ) and feed per tooth ( $f_z$ ) on surface hardness

As for the effect of feed per tooth on hardness, the results of this work are similar to those obtained by El-Wardany et al. [13]. The reduction in feed per tooth ( $f_z$ ) implied an increase in hardness close to the machined surface. The ANOVA showed no influence of cutting speed on hardness within the range investigated.

### 3.8 Influence of cutting parameters on residual stress

The ANOVA (Table 11 in the “Appendix”) shows that cutting speed ( $v_c$ ) exerted the strongest effect on longitudinal residual stress. Figure 19 shows the behavior of this output variable against this parameter.

The results obtained by Ramesh et al. [24] are consistent with those of the present work. In their work, they also showed that cutting speed ( $v_c$ ) was the parameter that exerted the

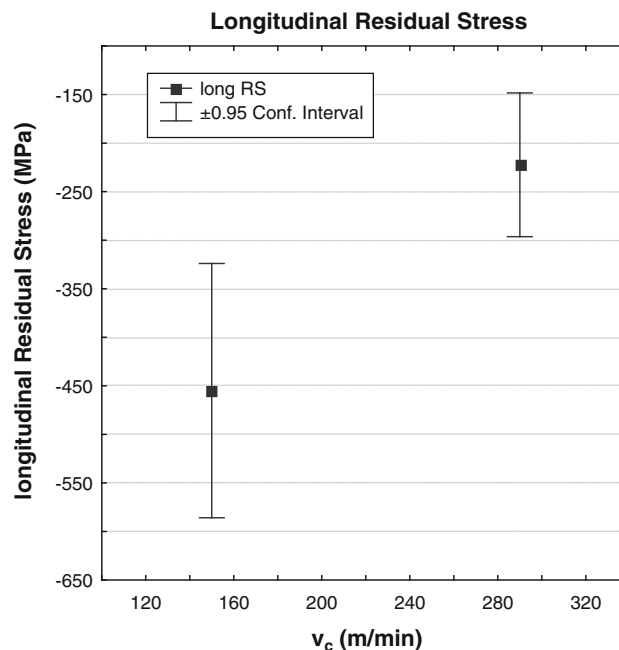


**Fig. 19** Influence of cutting speed ( $v_c$ ) on longitudinal residual stress

strongest effect on longitudinal residual stress and that the values were in the range of  $-700$  to  $-250$  MPa. These values are close to those found in this study, which were between  $-600$  and  $-150$  MPa.

At  $v_c = 150$  m/min, mechanical effects are predominant and longitudinal residual stresses are more compressive. Increasing the cutting speed generates a larger amount of heat, which reduces the mechanical effects and results in less compressive residual stresses, as shown in Fig. 19.

Yeo and Ong [36] demonstrated the correlation between cutting temperature and chip color. In their experiments, the color of the chip was silver at low cutting speeds ( $v_c$ ), gradually changing to golden, brown, violet and finally black as the  $v_c$  increased. In this work, the color of the chip was bright gold at  $v_c = 150$  m/min and bright purple at  $v_c = 300$  m/min, indicating that the temperature was higher.

The strongest effect on transverse residual stress was caused by feed per tooth ( $f_z$ ), according to the ANOVA (Table 11 in the “Appendix”). Figure 20 shows the behavior of this output variable against this parameter.

At very low  $f_z$ , the hardening effect predominated due to the effects of chip thickness and, therefore, the residual stress was more compressive. Increasing the feed intensified the thermal effects, causing the residual stress to be less compressive. These results are consistent with those of Sasahara [26], who stated that increasing the feed causes a tendency for the formation of tensile residual stress.

White layer thickness, surface hardness and compressive residual stresses depend, on the one hand, on hardening (cold working) due to the mechanical effect of the cutting

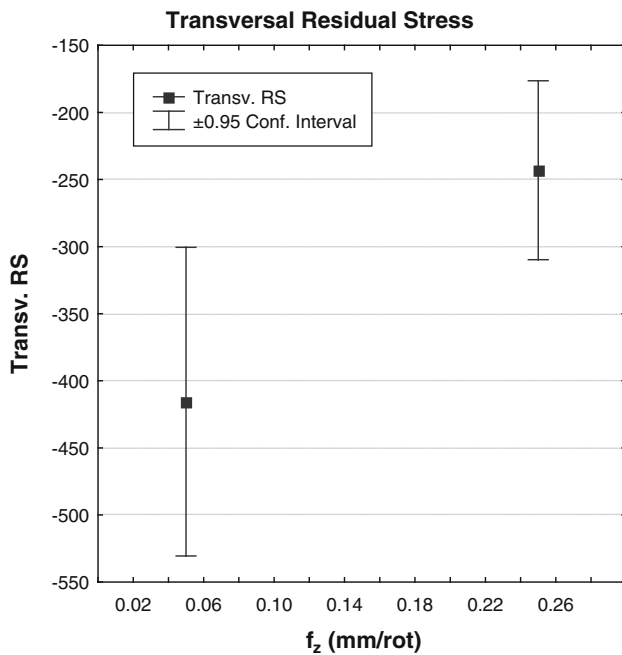


**Fig. 20** Influence of feed per tooth ( $f_z$ ) on transverse residual stress

tool. On the other hand, higher cutting speeds cause the temperature to rise. Under the conditions of this study, the thermal effect was not strong enough to affect the white layer and hardness.

The thermal effect caused by the increase in cutting speed was only noted in the residual stresses. This effect is analogous to what occurs in the heat treatment of hardened steels. For example, the hardening caused by cold rolling, in addition to augmenting the hardness, also augmented the compressive residual stresses on the surface.

Tempering at lower temperatures relieves residual stresses, and at higher temperatures reduces hardness due to recovery and recrystallization phenomena. Whereas the hardness variation and the formation of white layer have a similar origin (hardening), this analogy may be useful for the understanding of the mechanical effect of machining (due to the parameters  $a_e$ ,  $a_p$  and  $f_z$ ) and the thermal effect of machining (due to increased  $v_c$ ).

## 4 Conclusions

Based on the ANOVA of the effects of cutting parameters on surface integrity, it can be concluded that under conditions similar to those used in this work:

1. From the standpoint of machining conditions, the surface texture was determined by the machining parameters of work engagement ( $a_e$ ) and feed per tooth ( $f_z$ ).

2. In applications that involve contact between two bodies, the control of cutting parameters determines the roughness parameters. It was found that:

- 2.1. The cutting parameter of working engagement ( $a_e$ ) affected the roughness parameters  $S_a$ ,  $S_q$ ,  $S_z$ ,  $S_{sk}$ ,  $S_{ku}$ ,  $S_k$ ,  $S_{pk}$  and  $S_{vi}$ , while the feed per tooth ( $f_z$ ) affected the  $S_{tr}$ . The depth of cut ( $a_p$ ), similarly to  $v_c$ , exerted no significant influence on the parameters of 3D roughness.
- 2.2. When low values of  $a_e$  were used, low values of amplitude parameters ( $S_a$ ,  $S_q$ ,  $S_z$ ) were obtained (smoother surfaces).

3. The cavities with circular geometry, conditions 10 and 11, were obtained when the values of work engagement ( $a_e$ ) approached the feed per tooth ( $f_z$ ) values.
4. With regard to the mechanical and metallurgical properties, this work suggests that the values of white layer thickness, hardness and residual stresses result from a balance between mechanical (cold hardening) and thermal (temperature produced by the cutting speed) effects, indicating that:

- 4.1. The increase in depth of cut ( $a_p$ ) augmented the white layer thickness and surface hardness, while the increase in feed per tooth ( $f_z$ ) caused these parameters to decrease.
- 4.2. The increase in cutting speed ( $v_c$ ) induced less compressive residual stresses.
- 4.3. The work engagement ( $a_e$ ) showed no significant influence on white layer thickness, hardness and longitudinal and transverse residual stress.

5. HSM milling alters the integrity of the surface of hardened AISI H13 steel, even when fresh tools are used.

**Acknowledgments** The authors are indebted to Villares Metals for donating the AISI H13 steel, Brasimet for the heat treatments, Sandvik for donating the tools and tool holder, the Institute of Aeronautical Technology (ITA) for conducting preliminary tests, the Brazilian–German Institute of Technology (ITBA) for loaning the use of a Deckel Maho machine tool, the Federal University of Uberlândia (UFU) for the 3D roughness measurements and the Institute for Energy and Nuclear Research (IPEN) for the residual stress measurements.

## Appendix

This paper analyzed only the influence of the cutting parameter with the strongest statistical effect on the roughness parameter.

See Table 5, 6, 7, 8, 9, 10, 11 and 12.

**Table 5** ANOVA of amplitude parameters

	SS	df	MS	F	p
ANOVA var: $S_a$					
(1) $v_c$	0.00013	1	0.00013	0.019	0.892933
(2) $a_p$	0.13524	1	0.13524	20.627	0.001895
(3) $a_e$	29.68343	1	29.68343	4,527.458	0.000000
(4) $f_z$	0.04442	1	0.04442	6.774	0.031481
$1 \times 2$	0.00025	1	0.00025	0.038	0.850622
$1 \times 3$	0.11816	1	0.11816	18.023	0.002817
$1 \times 4$	0.05629	1	0.05629	8.585	0.018996
Error	0.05245	8	0.00656		
Total SS	30.09036	15			
ANOVA var: $S_q$					
(1) $v_c$	0.01097	1	0.01097	1.245	0.296981
(2) $a_p$	0.13377	1	0.13377	15.173	0.004575
(3) $a_e$	39.59241	1	39.59241	4,490.749	0.000000
(4) $f_z$	0.02950	1	0.02950	3.346	0.104773
$1 \times 2$	0.00589	1	0.00589	0.668	0.437367
$1 \times 3$	0.08396	1	0.08396	9.523	0.014983
$1 \times 4$	0.06213	1	0.06213	7.047	0.029051
Error	0.07053	8	0.00882		
Total SS	39.98916	15			
ANOVA var: $S_z$					
(1) $v_c$	3.3581	1	3.3581	1.7258	0.225374
(2) $a_p$	1.8701	1	1.8701	0.9611	0.355635
(3) $a_e$	500.7525	1	500.7525	257.3447	0.000000
(4) $f_z$	7.9948	1	7.9948	4.1086	0.077219
$1 \times 2$	1.1503	1	1.1503	0.5911	0.464072
$1 \times 3$	0.1351	1	0.1351	0.0694	0.798860
$1 \times 4$	0.1871	1	0.1871	0.0961	0.764446
Error	15.5668	8	1.9458		
Total SS	531.0145	15			

**Table 6** ANOVA of amplitude distribution parameters

	SS	df	MS	F	p
ANOVA var: $S_{sk}$					
(1) $v_c$	0.028249	1	0.028249	1.32836	0.282371
(2) $a_p$	0.023570	1	0.023570	1.10833	0.323202
(3) $a_e$	0.567725	1	0.567725	26.69608	0.000856
(4) $f_z$	0.193490	1	0.193490	9.09847	0.016651
$1 \times 2$	0.005458	1	0.005458	0.25663	0.626110
$1 \times 3$	0.021047	1	0.021047	0.98968	0.348955
$1 \times 4$	0.006002	1	0.006002	0.28225	0.609660
Error	0.170130	8	0.021266		
Total SS	1.015670	15			
ANOVA var: $S_{ku}$					
(1) $v_c$	0.040000	1	0.040000	2.68231	0.140103
(2) $a_p$	0.207025	1	0.207025	13.88265	0.005822
(3) $a_e$	0.705600	1	0.705600	47.31601	0.000127
(4) $f_z$	0.105625	1	0.105625	7.08298	0.028744
$1 \times 2$	0.000400	1	0.000400	0.02682	0.873968
$1 \times 3$	0.050625	1	0.050625	3.39480	0.102651
$1 \times 4$	0.006400	1	0.006400	0.42917	0.530778
Error	0.119300	8	0.014913		
Total SS	1.234975	15			

**Table 7** ANOVA of functional parameters

	SS	df	MS	F	p
ANOVA var: $S_{pk}$					
(1) $v_c$	0.54538	1	0.54538	0.9956	0.347589
(2) $a_p$	0.49280	1	0.49280	0.8996	0.370644
(3) $a_e$	84.28158	1	84.28158	153.8621	0.000002
(4) $f_z$	1.78757	1	1.78757	3.2633	0.108475
1 × 2	1.17289	1	1.17289	2.1412	0.181541
1 × 3	1.61671	1	1.61671	2.9514	0.124127
1 × 4	0.16646	1	0.16646	0.3039	0.596509
Error	4.38219	8	0.54777		
Total SS	94.44559	15			
ANOVA var: $S_k$					
(1) $v_c$	4.1514	1	4.1514	4.6109	0.064044
(2) $a_p$	3.0888	1	3.0888	3.4307	0.101132
(3) $a_e$	143.7002	1	143.7002	159.6059	0.000001
(4) $f_z$	3.1773	1	3.1773	3.5290	0.097120
1 × 2	0.5513	1	0.5513	0.6123	0.456448
1 × 3	0.5738	1	0.5738	0.6373	0.447732
1 × 4	0.9168	1	0.9168	1.0183	0.342469
Error	7.2028	8	0.9003		
Total SS	163.3623	15			
ANOVA var: $S_{vi}$					
(1) $v_c$	0.000036	1	0.000036	0.5287	0.487869
(2) $a_p$	0.000006	1	0.000006	0.0944	0.766473
(3) $a_e$	0.010430	1	0.010430	154.4641	0.000002
(4) $f_z$	0.000570	1	0.000570	8.4421	0.019724
1 × 2	0.000000	1	0.000000	0.0016	0.969420
1 × 3	0.000736	1	0.000736	10.8969	0.010842
1 × 4	0.000000	1	0.000000	0.0041	0.950624
Error	0.000540	8	0.000068		
Total SS	0.012318	15			

**Table 8** ANOVA of spatial parameters

	SS	df	MS	F	p
ANOVA var: $S_{tr}$					
(1) $v_c$	0.003508	1	0.003508	65.0090	0.000041
(2) $a_p$	0.003531	1	0.003531	65.4488	0.000040
(3) $a_e$	0.004125	1	0.004125	76.4489	0.000023
(4) $f_z$	0.006985	1	0.006985	129.4542	0.000003
1 × 2	0.003609	1	0.003609	66.8884	0.000037
1 × 3	0.004587	1	0.004587	85.0083	0.000016
1 × 4	0.002696	1	0.002696	49.9708	0.000105
Error	0.000432	8	0.000054		
Total SS	0.029472	15			

**Table 9** ANOVA of white layer

	SS	df	MS	F	p
ANOVA var: white layer					
(1) $v_c$	0.01690	1	0.01690	0.07749	0.787791
(2) $a_p$	12.96000	1	12.96000	59.42228	0.000057
(3) $a_e$	2.85610	1	2.85610	13.09537	0.006795
(4) $f_z$	8.29440	1	8.29440	38.03026	0.000269
1 × 2	0.40960	1	0.40960	1.87804	0.207776
1 × 3	1.82250	1	1.82250	8.35626	0.020177
1 × 4	14.59240	1	14.59240	66.90692	0.000037
Error	1.74480	8	0.21810		
Total SS	42.69670	15			

**Table 10** ANOVA of surface hardness

	SS	df	MS	F	p
ANOVA var: microhardness					
(1) $v_c$	3,460.27	1	3,460.27	8.79040	0.018012
(2) $a_p$	21,321.31	1	21,321.31	54.16421	0.000079
(3) $a_e$	62.40	1	62.40	0.15853	0.700929
(4) $f_z$	11,010.41	1	11,010.41	27.97062	0.000738
1 × 2	4.29	1	4.29	0.01090	0.919402
1 × 3	1,689.07	1	1,689.07	4.29087	0.072067
1 × 4	19,770.52	1	19,770.52	50.22461	0.000103
Error	3,149.14	8	393.64		
Total SS	60,467.42	15			

**Table 11** ANOVA of residual stress

	SS	df	MS	F	p
ANOVA var: longitudinal residual stress					
(1) $v_c$	216,331.1	1	216,331.1	5,281.701	0.000000
(2) $a_p$	2,146.1	1	2,146.1	52.398	0.000089
(3) $a_e$	39,049.6	1	39,049.6	953.392	0.000000
(4) $f_z$	89,967.0	1	89,967.0	2,196.535	0.000000
1 × 2	29,478.1	1	29,478.1	719.704	0.000000
1 × 3	65,545.4	1	65,545.4	1,600.284	0.000000
1 × 4	0.2	1	0.2	0.005	0.943519
Error	327.7	8	41.0		
Total SS	442,845.2	15			
ANOVA var: transverse residual stress					
(1) $v_c$	56,566.9	1	56,566.9	1,144.777	0.000000
(2) $a_p$	9,829.0	1	9,829.0	198.916	0.000001
(3) $a_e$	15,874.8	1	15,874.8	321.267	0.000000
(4) $f_z$	118,960.9	1	118,960.9	2,407.481	0.000000
1 × 2	427.0	1	427.0	8.642	0.018719
1 × 3	25,208.2	1	25,208.2	510.154	0.000000
1 × 4	68,658.4	1	68,658.4	1,389.480	0.000000
Error	395.3	8	49.4		
Total SS	295,920.5	15			

**Table 12** Results of measurements of 3D parameter

Condition	1	1	4	4	6	6	7	7	10	10	11	11	13	13	16	16	53
Sample	41	47	40	45	42	44	43	46	48	55	51	56	50	54	49	53	
$S_a$	0.696	0.694	0.765	0.827	3.620	3.460	3.430	3.400	0.983	0.966	0.797	0.689	3.690	3.940	3.330	3.340	
$S_q$	0.860	0.837	0.945	1.030	4.310	4.110	4.020	3.970	1.170	1.170	0.988	0.841	4.220	4.480	3.930	3.970	
$S_p$	3.850	6.350	5.130	4.210	12.400	12.800	11.400	12.100	5.310	5.490	3.970	4.700	11.200	14.700	12.600	12.200	
$S_v$	2.380	5.250	2.620	4.390	6.470	8.180	5.860	6.160	3.970	3.660	3.850	3.360	6.530	10.000	7.510	7.870	
$S_t$	6.230	11.600	7.750	8.610	18.900	21.000	17.200	18.300	9.280	9.160	7.810	8.060	17.700	24.700	20.100	20.100	
$S_{sk}$	0.419	-0.012	0.497	0.299	0.615	0.562	0.680	0.705	0.078	0.128	-0.113	0.082	0.525	0.263	0.496	0.546	
$S_{ku}$	2.690	2.440	2.930	2.710	2.250	2.300	2.250	2.250	2.250	2.510	2.740	2.580	1.990	1.830	2.270	2.350	
$S_z$	5.910	7.920	7.070	7.290	17.900	19.500	16.900	16.500	8.250	8.800	7.350	7.300	17.100	22.000	19.700	19.800	
$S_{Hip}$	1.520	1.530	1.650	1.770	8.610	7.870	7.760	7.740	2.200	2.130	1.710	1.470	8.380	9.230	7.630	7.520	
$S_{mmr}$	0.002	0.005	0.003	0.004	0.006	0.008	0.006	0.006	0.004	0.004	0.004	0.003	0.007	0.010	0.008	0.008	
$S_{mvr}$	0.004	0.006	0.005	0.004	0.012	0.013	0.011	0.012	0.005	0.005	0.004	0.005	0.011	0.015	0.013	0.012	
$S_{pc}$	0.000	0.000	0.000	0.000	0.250	0.250	0.250	0.250	0.000	0.000	0.000	0.000	0.250	0.250	0.250	0.250	
$S_{ds}$	4.449	3.981	5.087	5.069	4.773	4.216	4.858	5.116	3.897	4.399	3.439	3.382	3.070	3.453	2.904	3.407	
$S_r$	0.043	0.042	0.040	0.030	0.100	0.102	0.101	0.100	0.055	0.047	0.157	0.183	0.109	0.108	0.116	0.117	
$S_{a1}$	0.011	0.010	0.010	0.007	0.025	0.025	0.025	0.025	0.012	0.010	0.018	0.012	0.026	0.027	0.026	0.026	
$S_{td}$	71.5	83.5	85.0	85.0	89.0	89.0	89.0	88.5	63.5	63.5	68.0	68.0	73.5	63.5	68.0	68.0	
$S_{fd}$	2.450	2.470	2.440	2.410	2.300	2.200	2.280	2.260	2.460	2.470	2.490	2.480	2.310	2.280	2.380	2.380	
$S_{dq}$	0.199	0.226	0.230	0.237	0.236	0.194	0.183	0.187	0.296	0.349	0.250	0.276	0.205	0.254	0.290	0.288	
$S_{sc}$	0.260	0.301	0.293	0.289	0.294	0.229	0.242	0.242	0.384	0.414	0.353	0.372	0.287	0.330	0.402	0.394	
$S_{dr}$	1.890	2.410	2.510	2.640	2.430	1.790	1.610	1.680	4.070	5.540	2.930	3.510	1.990	2.980	3.900	3.870	
$S_k$	2.140	2.440	2.440	2.620	9.540	9.280	7.010	6.300	3.660	3.240	2.560	2.260	7.450	11.100	9.490	9.140	
$S_{pk}$	0.984	0.529	1.210	1.130	5.420	5.210	6.660	7.090	0.782	1.010	0.808	0.745	6.520	3.700	4.380	4.940	
$S_{vk}$	0.450	0.561	0.397	0.628	0.207	0.993	0.377	0.409	0.540	0.741	0.920	0.565	0.445	1.280	0.745	1.050	
$S_{r1}$	14.70	7.71	12.50	13.40	24.60	21.10	29.60	32.80	6.55	10.50	9.57	9.74	32.70	22.40	20.30	21.40	
$S_{r2}$	92.40	92.40	94.30	92.00	99.50	97.50	97.70	98.20	95.70	93.00	89.40	91.00	98.50	97.40	97.50	96.90	
$S_{bi}$	0.380	0.167	0.277	0.432	1.040	0.821	1.100	0.879	0.343	0.332	0.415	0.255	1.210	0.603	0.709	0.813	
$S_{ci}$	1.780	1.520	1.760	1.720	1.880	1.870	1.890	1.900	1.550	1.590	1.510	1.580	1.800	1.580	1.760	1.810	
$S_{ji}$	0.086	0.104	0.073	0.086	0.040	0.042	0.034	0.030	0.086	0.095	0.113	0.103	0.033	0.051	0.052	0.056	



## References

1. Abbott E, Arbor A (1941) Instrument for recording or measuring surface irregularities. USA, patented 2.240.278
2. American Society of Mechanical Engineers (2003) ASME B46.1-2002: surface texture (surface roughness, waviness and lay). American Society of Mechanical Engineers, New York, p 98
3. Axinte DA, Dewes RC (2002) Surface integrity of hot work tool steel after high speed milling-experimental data and empirical model 127:325–335
4. Bayer RG (1994) Mechanical wear prediction and prevention. Marcel Dekker, New York, p 657p
5. Boeschoten F, Van Der Held EFM (1957) The thermal conductance of contacts between aluminum and other metals. *Physical* 23:37–44
6. Bosheh SS, Mantivega PT (2006) White layer formation in hard turning of H13 tool steel at high cutting speed using CBN tooling. *Int J Mach Tools Manuf* 46(2):225–233
7. Braghini Jr A (2002) Methodology for choice of cutting fluid non aggressive to environment to applications in metals machining, 2002. Thesis (doctorate), Engineering School of São Carlos, University of São Paulo, São Carlos, p 248
8. Brazilian Technical Standard Association (2002) Geometrical product specification (GPS)—surface texture: profile method—terms, definitions and surface texture parameters. NBR ISO 4287:2002, Rio de Janeiro
9. Cao BY, Chen M, Guo ZY (2006) Effect of surface roughness on gas flow in microchannels by molecular dynamics simulation. *Int J Eng Sci* 44:927–937
10. Chevrier P, Tidu A, Bolle B, Cezard P, Tinnes JP (2003) Investigation of surface integrity in high speed end milling of a low alloyed steel. *Int J Mach Tools Manuf* 43:1135–1142
11. Dewes RC, Chua KS, Newton PG, Aspinwall DK (1999) Temperature measurement when high speed machining hardened mould/die steel 92–93:293–301
12. Diniz AE, Marcondes FC, Coppini NL (2000) Technology machining of metals 2nd edition. Publisher Artiber, São Paulo, p 244
13. El-Wardany TI, Kishawy HA, Elbestawi MA (2000) Surface integrity of die material in high speed hard machining, part 1: micrographical analysis. *Trans ASME* 122:620–631
14. Fallböhmer P, Rodrigues CA, Özel T, Altan T (2000) High-speed machining for cast iron and alloy steel for die and mold manufacturing. *J Mater Process Tech* 98:104–115
15. Field M, Kahles JF (1971) Review of surface integrity of machine components. *Annals CIRP* 20(2):153–162
16. Field M, Kahles JF, Cammett JT (1972) Review of surface integrity of machine components. *Annals CIRP* 20(2):219–238
17. Firestone FA, Arbor A, Durbin M (1934) Apparatus for determining roughness of surfaces. USA Pat 1(976):337
18. Griffiths B (2001) Manufacturing surface technology, 1st edn. Penton Press, London, p 237
19. Hioki D (1998) Hard turning of 100Cr6 steel with PCBN. Dissertation (Masters), Federal University of Santa Catarina, Florianópolis, p 164
20. Hutchings IM (1992) Tribology: friction and wear of engineering material, 1st edn. Edward Arnold, London, p 273
21. Magri ML, Diniz AE, Button ST (2012) Influence of surface topography on the wear of hot forging dies. *Int J Adv Manuf Technol* 1–13. doi:10.1007/s00170-012-4185-1
22. Mancuso RD (2005) Tribological coating Cr–N and plasma nitriding for improvement of cavitation erosion resistance of a carbon steel ABNT 1045: a topographical approach. Thesis (doctorate), Federal University of Minas Gerais, Brazil, p 305
23. Poulachon G, Albert A, Schluraff M, Jawahir IS (2005) An experimental investigation of work material microstructure effects on white layer formation in PCBN hard turning. *Int J Mach Tools Manuf* 45(2):211–218
24. Ramesh A, Melkote SN, Allard LF, Riester L, Watkins TR (2005) Analysis of white layers formed in hard turning of AISI 52100 steel. *Mater Sci Eng* 39:88–97
25. Rech J, Moisan A (2003) Surface integrity in finish hard turning of casehardened steels. *Int J Mach Tools Manuf* 43:543–550
26. Sasahara H (2005) The effect on fatigue life of residual stress and surface hardness resulting from different cutting conditions of 0.45 % C steel. *Int J Mach Tools Manuf* 45(2):131–136
27. Sandvik Coromant (2006) Main catalogue. São Paulo, p 1038
28. Sandvik Coromant (2000) Fabricación de Moldes y Matrices, Sweden (manual C-1120:2SPA)
29. Starr AT, Reeve TC (1971) Electrical filters. USA, patented 3.555.439
30. Stout KJ (1998) Engineering surfaces—a philosophy of manufacture (a proposal for good manufacturing practice). *Proc Inst Mech Eng* 212:169–174
31. Stout KJ, Blunt LA (2001) Contribution to the debate on surface classifications—random, systematic, unstructured, structured and engineered. *Int J Mach Tools Manuf* 41:2039–2044
32. Trumpold H, Heldt E (1997) Why filtering surface profiles? *Int J Mach Tools Manuf* 38:639–646
33. Uppal AH, Probert SD (1970) Electrical resistance of single contacts under normal dynamic forces. *Wear* 15(4):271–280
34. Urbanski JP, Koshy P, Dewes RC, Aspinwall DK (2000) High speed machining of moulds and dies for net shape manufacture. *Mater Des* 21:395–402
35. Whitehouse DJ, Mowbray M (1970) Compensation for phase distortion in surface profile measuring apparatus. USA, patented 3.543.571
36. Yeo SH, Ong SH (2000) Assessment of thermal effects on chip surface. *J Mater Process Technol* 98:317–321